Quantitative contribution of resistance sources of components to stack performance for planar solid oxide fuel cells

CrossMark

Le Jin, Wanbing Guan [1], Xiao Ma, Huijuan Zhai, Wei Guo Wang*

Ningbo Institute of Material Technology & Engineering, Chinese Academy of Sciences, 519 Zhuangshi Road, Ningbo 315201, China

HIGHLIGHTS

- ASRs of components inside stack were quantitatively measured.
- ASRs of cell and cathodic contact account for near 100% of that of the overall stack.
- Increasing cell ASR was the main reason for stack degradation as cathode contacted well.
- Anodic contact cannot be ignored for stack degradation.

ARTICLE INFO

ABSTRACT

This study detects the resistance that influences the stack performance of SOFCs with composition of Ni-YSZ/YSZ/LSC-YSZ and investigates the variation patterns of the resistances of the stack repeating unit (SRU) during operation and their quantitative contributions to its performance at 700 °C, 750 °C and 800 °C. The results indicate that when the cell cathode contacts the interconnect well, the cell resistance accounts for 70.1–79.7% of that of the SRU, and the contact resistance (CR) between the cathode current-collecting layer (CCCL) and the interconnect accounts for 20.0–28.9%. The CR between the anode current-collecting layer (ACCL) and the interconnect together with the resistance of the interconnect can be neglected during instantaneous I–V testing. When the stack is discharged at constant current for 600 h, cell resistance increases by 28.3%, accounting for 93.3% of the SRU degradation, the anodic CR increases by 36.4%, accounting for 6.7% of the SRU degradation, and the resistances of the cathode contact and its neighbor interconnect remain unchanged. Therefore, the increase of the cell resistance is the main reason causing the SRU degradation, and the anodic contact is also an influencing factor that cannot be neglected during stable operation.

1. Introduction

Solid oxide fuel cells (SOFCs) are highly efficient energy transformation device. In order to obtain applicable electric power, multiple unit cells (UCs) with limited voltage need to be connected in series to form a stack [1]. In order to satisfy the requirement of commercial application, the SOFC stack should not only have high output power, but also satisfy the requirement of an operation time of over 40,000 h [2]. Therefore, the stable operation of stacks is a premise for the commercialization of SOFCs. There have been numerous studies on the causes of the stack degradation. The causes influencing the operating stability of the stacks include sealing, stack components and the interfacial contact between the components [3–7]. If a stack is not properly sealed and gas leakage exists, the voltage will drop down during the operation of the stack, resulting in serious degradation of the stack performance [8,9,10]. According to the structure of SOFC stack [11], the component resistances of the stack are mainly from the cells and the interconnects. The interfacial resistance between the components comes from the interfacial contact between the anode and the interconnect and between the cathode and the interconnect. Thus, the increase of the cell resistance and the interfacial contact resistances (CRs) between its components can also cause the stack degradation. Therefore, in order to decrease the stack degradation and to increase its service life, researchers focus on the development of sealing materials [12,13], improvement of the cell performance [14,15], and the protective treatment of the interconnect [16–18]. However, even with excellent sealing performance and acceptable oxidation resistance of the interconnect at high

* Corresponding author. Tel.: +86 574 8791 1363.
E-mail addresses: guanwanbing@gmail.com (W. Guan), wgwang@nimte.ac.cn, april.jin@gmail.com (W.G. Wang).
[1] Tel.: +86 574 8668 5137.

temperature, the stack degradation reported in literature are still high, with some of them reaching 10%/1000 h [19,20]. In this regard, researches revealed that the interfacial contact was also an important factor influencing the stack degradation [21]. Therefore, by improving the interfacial contact, the stack degradation can be further reduced to approximately 2%/1000 h [22,23], which, however, is still high and cannot satisfy the requirements of commercialization. Therefore, further reduction of the stack degradation rate to the requirements of commercialization is an urgent problem that needs to be solved.

In this regard, the resistance sources of the stack under the condition of excellent sealing performance and proper interfacial contact between components should be clarified (the variation of the component resistance in stack operation), for the purpose of further countermeasures. Researchers [24,25] measured the resistance of the interconnects with protective coating under stack operation. The results indicated that the high-temperature resistance of the corresponding interconnects is stable under the working temperature of SOFC. It seemingly did not influence the stack performance in the operation time. Therefore, the concerns gradually turned to the factors other than the interconnects in the stack, such as the interfacial contact [21,22,26−29]. In 2006, K. A. Nielsen [26] et al. measured quantitatively the interfacial CR during the stack operation. The results indicated that within the operation time of 1200 h, the interfacial CR between the interconnect and the CCCL increased continuously; the interfacial CR between the interconnect and the ACCL first decreased and then increased. The study reported the quantitative results of the interfacial CR under stable operation of the stack. However, the quantitative contribution of the interfacial CR to the stack performance was not obtained. Therefore, it is difficult to determine the role and effects of the interfacial contact in the complicated environment of stack operation. In this regard, our research group conducted extensive investigations on the factors which influence the stack performance at the early stage. Our results indicated that the interfacial contact between the interconnect and the cell cathode was the most important factor influencing the stack performance [21,22,30]. However, the quantitative contribution of the interfacial contact to the stack performance was not found, either, especially the quantitative variation patterns of the interfacial CR during the stack operation. Recently, researchers [27,28] measured the variation patterns of the interfacial CR between the interconnect and the cathode. The results indicated that the interfacial CR was closely related to external pressure and varied with the variation of temperature. It provided a reference in taking measures to decrease the interfacial CR, but still did not report the quantitative relationship between the interfacial CR and the stack performance. Neither was the variation of interfacial CR under stable operation conditions in long term involved. The operation environment of a stack is complicated, with numerous factors influencing its performance, including the interconnect, the interfacial contact and the cell itself [30−32]. For example, H. T. Lim [30] et al. investigated the cell degradation of an anode-supported SOFC. Their results indicated that the increase of resistance was an essential cause of the cell degradation. However, their study was limited to the cell itself, without concerning the correlation between the cell performance and the stack performance. Therefore, despite numerous studies on the factors influencing the stack performance, the factors investigated in the studies are similar. In addition, quantitative investigation on the correlation between various factors and the stack performance during its operation are still lacked. This study assembled stacks and measured the sources of internal resistance which influenced the stack performance (instantaneous discharge $I-V$ curve and long-term stable operation $V-t$ curve). A quantitative analysis on the patterns by which the resistance of every component influences the stack performance was also carried out, in order to provide a reference for the improvement of the service life for the SOFC stack.

2. Experimental methods

The unit cell (UC) used in the experiments was an anode-supported NiO-YSZ/YSZ/LSC cell. A 500 μm-thick anode of Ni/YSZ was tape casted as the supported substrate, and a 10 μm-thick active anode of Ni/YSZ and a 10 μm-thick electrolyte of YSZ were sprayed onto the supported substrate followed by sintering at 1350 °C for 3 h. A 25 μm-thick cathode of 50 wt.% $La_{0.6}Sr_{0.4}CoO_3$ (LSC) with the GDC interlayer was then sprayed on the electrolyte and fired at 1080 °C for 4 h. The cell size in the stack was 10 cm × 10 cm with an active area of about 63 cm^2. Cells were machined to the required size by laser cutting. For the complete contact between the cell electrodes and the metal interconnects, a coating of NiO with 130 μm thickness was screen printed on the cell anode and a coating of $(La_{0.75}Sr_{0.25})_{0.95}MnO_3$ (LSM) current-collecting layer of 250 μm-thick was screen printed on the cell cathode. Then, the components prepared by the method mentioned above were assembled into a 5-cell stack according to the schematic diagram shown in Fig. 1 [22]. In the stack, 430 ferritic stainless steel and $Al_2O_3−SiO_2−CaO$-based glass were applied as metal interconnect and sealant, respectively. In order to avoid the Cr element diffusion into the cell cathode, a kind of dual protective layer was sprayed onto the cathode side of interconnect, which was reported in our previous research [21,29]. And the performance of the sealing material can also be found in our previous literature [33]. The 5-cell stack includes 5 pieces of SRUs. A piece of SRU was consisted of a piece of UC and two pieces of neighboring interconnects in this work, as shown in Fig. 2. The SRUs in the stack were numbered 1#, 2#, 3#, 4# and 5#, respectively.

After assembled, the stack was placed into the heating furnace. The temperature was raised to 850 °C at the rate of 1 °C min^{-1}. The temperature was kept stable for 4 h and then decreased to the working temperature required by the experiments for analysis. Before testing, a certain quantity of nitrogen was fed into the anode for 5 min and then 1 L min^{-1} (SLM) of hydrogen was fed. After 10 min, 3 SLM of air was fed into the cathode. After 2 h of reduction
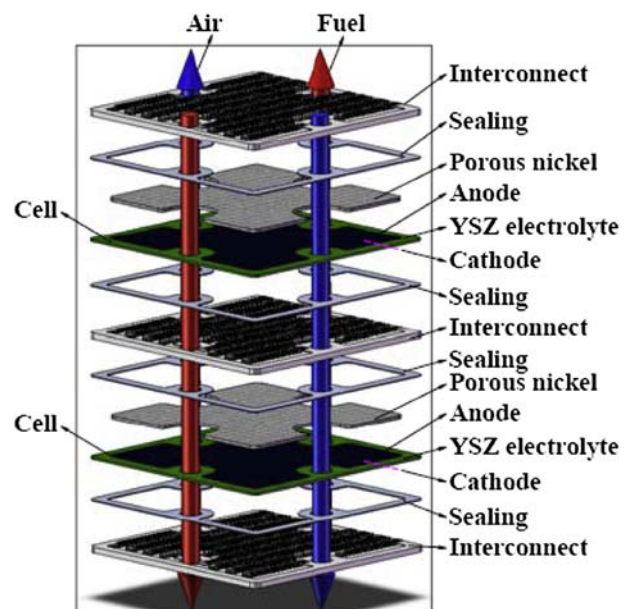

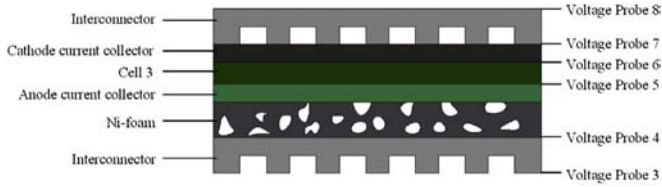**Fig. 1.** Schematic diagram of stack assembling.

Fig. 2. Schematic diagram of voltage leads on various locations in the SRU 3 #.

Fig. 3. Analog circuit of the components in the SRU 3#.

in the previously stated anode atmosphere, the tests required by the experiment could be carried out. After tests, the Hitachi S-4800 SEM was used in the observation of the cell microstructure.

During the tests, in order to quantitatively measure the resistance of the components in the SRUs, the voltage leads were led from the components and the SRU 3# in the middle of the stack was selected as the object of study for the quantitative analysis of the resistance sources of the components. The voltage leads on the both ends of each component in the SRU are shown in Fig. 2 and Table 1. Fig. 2 and Table 1 indicated that the voltage measured by the voltage leads 3—7 was the voltage of the both ends of SRU 3#; that of the leads 5—6 was the voltage of the both ends of UC 3#; that of the leads 6—7 was the voltage drop caused by the contact between the CCCL and the interconnect; that of the leads 4—5 was the voltage drop caused by the contact between the ACCL and the interconnect; that of the leads 3—4 was the voltage drop caused by the interconnect.

In Fig. 2, the resistance of the components in the SRU could be considered as a series of connected resistance including a voltage source. The analog circuit is shown in Fig. 3. In this research, the interconnect resistance is signified as R_{IC} (measured by leads 3—4); the sum of the resistance generated by the contact between the ACCL and the interconnect is abbreviated as anodic CR, shown as R_A (measured by leads 4—5); the internal resistance of the UC are shown as R_{cell} (measured by leads 5—6); the sum of the resistance generated by the contact between the CCCL and the interconnect is abbreviated as cathodic CR, shown as R_C (measured by leads 6—7). Fig. 3 indicates that the resistance of the components of the stack can be calculated using the ohmic equation, which was written as equations (1) and (2):

$$R_i = U_i/I \tag{1}$$

$$R_{cell} = (U_0 - U_{5-6})/I \tag{2}$$

In the equation (1), R_i is the resistance of interconnect, anodic and cathodic contact; U_i (U_{3-4}, U_{4-5}, U_{6-7}) is the voltage drop caused by interconnect, anodic and cathodic contact, respectively; I is the current. In the equation (2), U_0 is the open circuit voltage (OCV), U_{5-6} is the voltage of both ends of UC 3#. Therefore, during the stack operation, the corresponding resistance of the components can be calculated with the operation voltage between both ends of the stack components. Then, during the stack operation, the quantitative analysis can be conducted on the stack degradation according to the variation patterns of the resistance.

In Fig. 2, the voltage leads 3, 4, 7 and 8 were all welded to the groove of the corresponding gas pathway of the interconnects, and the voltage leads 5 and 6 were welded to the surface of the
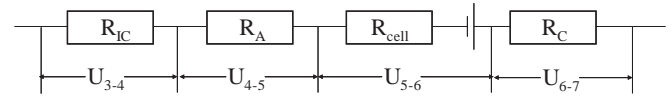
electrodes on both sides of the cell with platinum paste. The procedure is shown in Fig. 4 [34]. In order to prevent the short circuit between the leads on the electrode sides and the interconnects, which results in the test errors, the voltage leads on both sides of the cell electrodes were isolated from the interconnects by sealing materials.

3. Results and discussion

3.1. Quantitative contribution of resistance sources to stack output power density

During the stack operation, 3 SLM of hydrogen and 9 SLM of air were used as the fuel and oxidant gas. The performance of the stack and SRUs under different temperatures is shown in Figs. 5 and 6. In order to clearly compare the performance of the stack and the SRUs under different temperatures, the results shown in Figs. 5 and 6 are listed in Table 2. The data listed in Table 2 indicated that under the same operation temperature, the OCV and maximum output power density (MOPD) of each SRU were close. The MOPD of SRU 2# was slightly lower than that of other four SRUs. The difference came from the fact that the diffusion polarization of SRU 2 # in the stack was larger. But the ohmic resistance of SRU 2# was also close to that of other SRUs. Therefore, on the premise that the output performance of every SRU was similar, the SRU 3# in the middle of the stack was selected as the research object in the discussion below.

Fig. 7 is the I—V curve of SRU 3# and its corresponding UC under different temperatures. The resistance of SRU 3# and UC 3# under different temperatures was obtained by linear fitting of I—V curves. The slopes of the fitted line in Fig. 7a) under 700 °C, 750 °C and 800 °C were 0.915, 0.717 and 0.492, respectively. If the slope of the fitted line is k_i, the voltage drop in a certain current range (ΔI_i) is ΔU_i, and the resistance of component i is R_i, then, the following equation can be obtained:

$$k_i = \frac{\Delta U_i}{\Delta I_i} = R_i \tag{3}$$

That is, the slope of the fitted line is the resistance of the SRU. The resistances of the SRU under different temperatures are listed in Table 3. The results indicated that the area specific resistance (ASR) of the SRU under 700 °C, 750 °C and 800 °C was 0.915 Ω cm^2, 0.717 Ω cm^2 and 0.492 Ω cm^2, respectively. With the increase of the working temperature, the ASR of the SRU decreased significantly. According to the same fitting method, the fitted results of the UC are shown in Fig. 7b). The results showed that the slopes of the I—V curve of the UC under 700 °C, 750 °C and 800 °C were 0.729, 0.556 and 0.345, i.e. the ASR of the UC was 0.729 Ω cm^2, 0.556 Ω cm^2 and 0.345 Ω cm^2, respectively. The results are coherent to the findings in the reference [35]. With the increase of the working temperature, the ASR of the UC decreased significantly. Accordingly, it can be found that the ASR of the UC accounted for 79.7%, 77.5% and 70.1% of that of the SRU at the temperature of 700 °C, 750 °C and 800 °C, respectively.

The cathodic CR was measured by the voltage leads 6—7, the anodic CR by leads 4—5, and the interconnect resistance by leads 3—4. As the ASR values of the cathodic contact, anodic contact and interconnect were small, the voltage at both ends was small. Due to

Table 1
Voltage leads on both ends of the components of the SRU 3#.

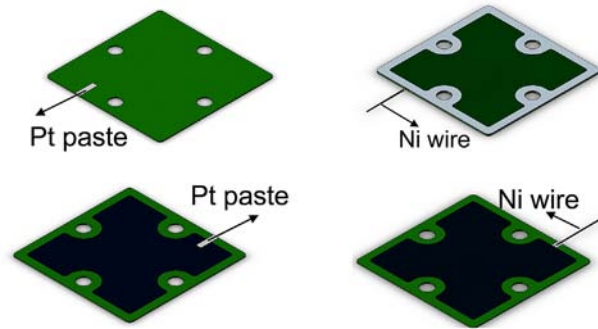| Component	SRU	UC	CCCL and contact	ACCL and contact	Interconnect
Voltage leads	3—7	5—6	6—7	4—5	3—4

Fig. 4. Schematic diagram of voltage leads 5 and 6 arranged on both sides of UC 3#.

the limit of the precision of the apparatus, the voltage was unable to be measured directly during the I–V curve discharging. Therefore, the voltage between both ends of the cathodic contact was obtained by the difference between the voltage values of the leads 5–6 and leads 5–7, and the voltage between both ends of the anodic contact was obtained by the difference between the voltage values of the leads 5–6 and leads 4–6.

$$U_{6-7} = U_{5-6} - U_{5-7} \tag{4}$$

$$U_{4-5} = U_{5-6} - U_{4-6} \tag{5}$$

Fig. 8 is the I–V curves between both ends of 5–6, 5–7 and 4–6. From Fig. 8a) and equation (4), the relationship between the voltage difference at both ends of 5–6 and 5–7, U_{5-6} and U_{5-7}, and the current could be obtained. That is, the I–V curves between the cathodic contact voltage and the current could be obtained, as shown in Fig. 9 a). Similarly, according to equation (5), the I–V curves between the anodic contact voltage and the current could be obtained, as shown in Fig. 9b). The curves under different temperatures in Fig. 9a) were linearly fitted. The slopes under 700 °C, 750 °C and 800 °C were 0.183, 0.154 and 0.142, respectively. The curves under different temperatures in Fig. 9b) were also linearly fitted. And the slopes under 700 °C, 750 °C and 800 °C had the same value of 0.006. With equation (3) and the slopes of curves in Fig. 7a and b, the ASR for the cathodic and anodic contact under different temperatures could be got, as listed in Table 3. The results indicated that under 700 °C, 750 °C and 800 °C, the cathodic CRs of the SRU were 0.183 Ω cm², 0.154 Ω cm² and 0.142 Ω cm², and the anodic CRs were 0.006 Ω cm², 0.006 Ω cm² and 0.006 Ω cm², respectively. The cathodic CR was coherent to the results reported by Tapobrata Dey et al. [28]. Due to the improvement of the interfacial contact, the anodic CR was smaller than that reported in Ref. [28]. The results indicated that with the increase of the working temperature, the cathodic CR of the SRU decreased significantly, while the anodic CR remained unchanged. Accordingly, it can be deduced that the cathodic CRs accounted for 20.0%, 21.5% and 28.9%, respectively. While the anodic CRs accounted for only 0.6%, 0.8% and 1.2%, respectively. The total resistance of the UC, the cathodic contact and the anodic contact was over or less than 100% due to the test errors of the apparatus. In general, the UC in the SRU was still the main factor determining the output power density, accounting for 70.1–79.7%. And the cathodic contact was the second factor, generally accounting for 20.0–28.9%. Obviously, the anodic contact could be ignored during the instantaneous I–V testing. Therefore, the key to further improvement of the output power density of the stack lies in the reduction of the internal resistance of the UC and the

improvement of the cathodic contact. However, the sources of the resistance of the UC need to be further studied.

3.2. Quantitative contribution of resistance sources to stack degradation

Under 700 °C, 2 SLM of hydrogen and 6 SLM of air were fed into the anode and cathode, respectively. Then, the stack was discharged at a certain constant current under stable operation. The variation voltage curves of the stack, SRU 3# and its corresponding UC 3# with time are shown in Fig. 10. Fig. 10a) indicated that when the stack was discharged at a constant current of 0.33 A cm⁻² (fuel utilization of about 36.6%), the degradation did not take place within 120 h of operation. After 120 h, the operation current density was raised to 0.40 A cm⁻²(fuel utilization of about 43.5%), the degradation reached 0.23%/100 h within 480 h Fig. 10b) is the variation voltage curve of the SRU 3# and its corresponding UC 3 # with time. Fig. 10b) indicated that the SRU 3# showed no degradation within 120 h in constant current discharge of 0.33 A cm⁻², while the corresponding UC 3# appeared a degradation rate of 0.16%/100 h. Within 480 h, the constant current discharge of 0.40 A cm⁻², the degradation rate of the SRU 3# reached 0.30%/ 100 h, and that of the corresponding UC was 0.28%/100 h. The degradation of the UC accounted for 93.3% of that of the SRU. Fig. 10 indicated as well that before and after the discharge, the OCV was both near 1.2 V and did not change. The previous studies of our group revealed that the results indicated a good sealing performance of the stack [21,22]. Therefore, the sealing performance
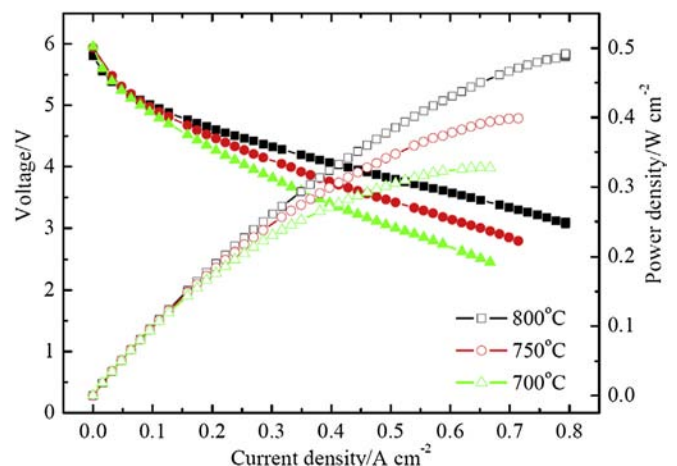

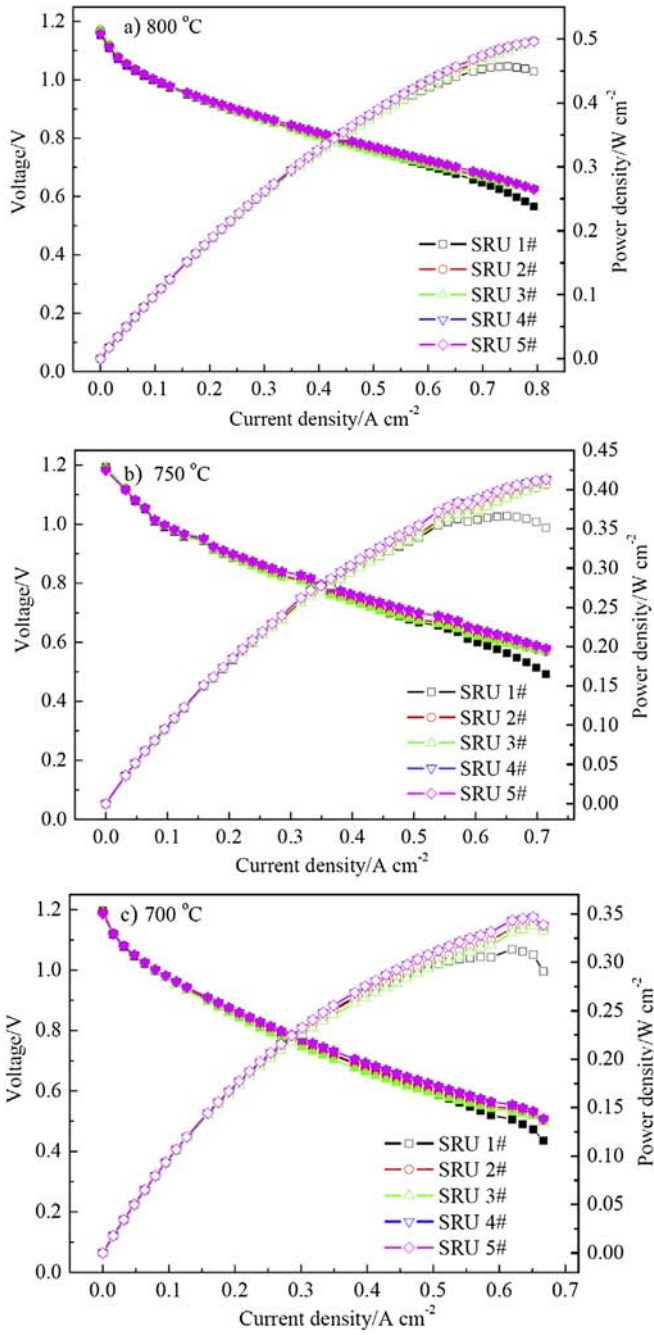**Fig. 5.** I–V curves of stack under different temperatures.

Fig. 6. I–V curves of the SRUs under different temperatures: (a) 800 °C, (b) 750 °C and (c) 700 °C.

Table 2
The OCV and MOPD of stack and SRUs under different temperatures.

Temperature	800 °C		750 °C		700 °C	
	OCV/V	MOPD/ W cm^{-2}	OCV/V	MOPD/ W cm^{-2}	OCV/V	MOPD/ W cm^{-2}
Stack	5.812	0.492	5.942	0.399	5.960	0.327
SRU 1#	1.153	0.449	1.194	0.351	1.197	0.291
SRU 2#	1.171	0.497	1.193	0.406	1.196	0.335
SRU 3#	1.173	0.495	1.192	0.406	1.190	0.332
SRU 4#	1.158	0.496	1.182	0.414	1.187	0.339
SRU 5#	1.158	0.496	1.182	0.414	1.187	0.339

that the interfacial CR between the interconnect and the cathode continuously increased within 1200 h. The reason could be the difference of the coatings of the interconnect or be the increase of the temperature inside the stack during the constant current operation [36,37]. During the constant current discharge, the temperature inside the stack increased, causing the increase of the conductivity of the LSM CCCL and the improvement of the cathodic contact, thus reducing the CR. However, when the temperature inside the stack was over 800 °C, the conductivity of the LSM did not increase with the increase of temperature [38]. Therefore, the cathodic CR showed that it decreased and then remained unchanged.

Fig. 11b) indicated that at the constant current discharge of 0.33 A cm^{-2}, the interconnect resistance was only 0.00058–0.001 Ω cm^2. The ASR value was very small in comparison with that

could not be a cause of the stack degradation. During the constant current discharge of the stack, the ASRs of the UC, cathodic contact, anodic contact and interconnect were measured and calculated according to the Ohm's law in equations (1) and (2). The results are shown in Fig. 11. And the resistances of different components in the stack at different moments were listed in Table 4.

Fig. 11a) indicated that during the constant current discharge, the initial cathodic CR reached 0.196 Ω cm^2, and dropped to 0.189 Ω cm^2 with the increase of the operation time, then remained relative stable after 190 h. The results indicated that during the discharge, the contact between the cathode and the interconnect was improved and then remained stable. The results are different from that reported by K. A. Nielsen et al. [26], whose findings were
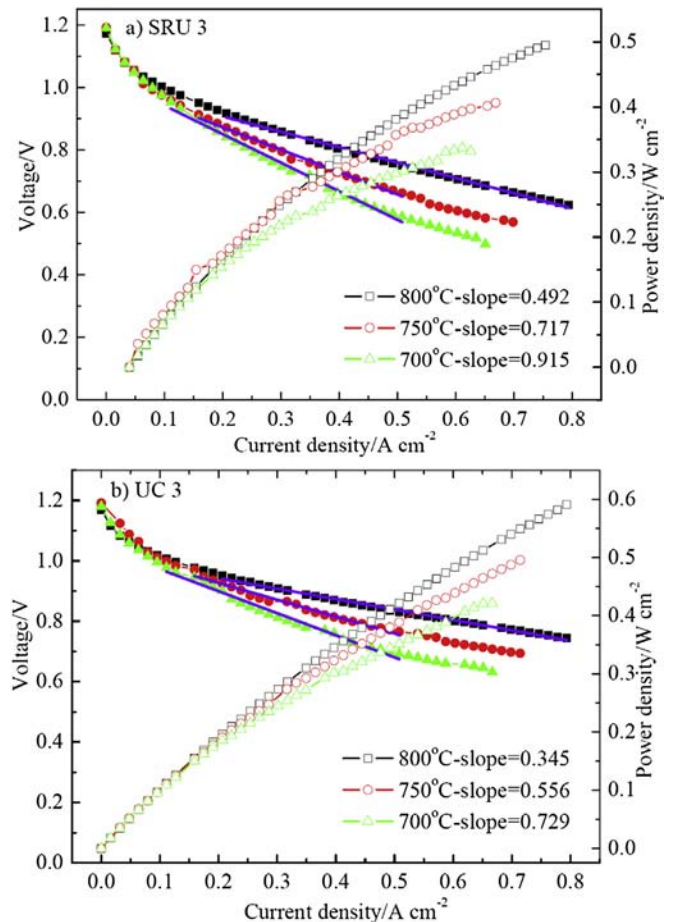

Fig. 7. I–V curves of the SRU and UC under different temperatures: (a) SRU and (b) UC.

Table 3
ASR of the stack components at the beginning and the end of discharge.

Temperature/°C	SRU 3#/Ω cm²	UC3#/Ω cm²	Cathodic contact/Ω cm²	Anodic contact/Ω cm²
700	0.915	0.729	0.183	0.006
750	0.717	0.556	0.154	0.006
800	0.492	0.345	0.142	0.006

of the whole unit in the stack, which could be neglected. The resistance of the interconnect remained unchanged for the whole time during the constant current operation. This result was coherent with the results reported in the reference [21]. Therefore, the interconnect barely had any influence on the stack degradation. Obviously, Fig. 11b) also showed that the anodic CR appeared a logarithmic increase with time within 600 h. The ASR value of the anodic CR rose from 0.0048 Ω cm² to 0.00907 Ω cm², by 88.96%. Therefore, with the prolongation of the operation time, the anodic CR would be a factor that could not be neglected influencing the stack degradation.

The results in Fig. 11c) indicated that the resistance of the UC at 0.33 A cm⁻² constant current discharge was 1.188 Ω cm² and increased to 1.191 Ω cm² within 120 h. When the current rose to 0.40 A cm⁻², the resistance of the UC dropped from 1.191 Ω cm² to 1.061 Ω cm², and then rose to 1.093 Ω cm². During the constant current discharge at 0.40 A cm⁻², the resistance of the UC rose by 3.02%. The results in the figure indicated that when the current rose from 0.33 A cm⁻² to 0.40 A cm⁻², the resistance of the UC dropped

due to the rise of internal temperature inside the stack caused by the increase of the current, according to our previous research [34]. The results in Fig. 11c) also indicated that the resistance of the SRU was 1.395 Ω cm² in the constant current discharge of 0.33 A cm⁻² and dropped to 1.392 Ω cm² within 120 h. When the current rose to 0.40 A cm⁻², the resistance of the SRU dropped from 1.392 Ω cm² to 1.260 Ω cm². The reduction of the ASR was mainly due to the decrease of the ASR of the UC itself. During the following 480 h of constant current discharge at 0.40 A cm⁻², the stack showed degradation and the ASR of the SRU rose gradually by 0.025 Ω cm² to 1.285 Ω cm².

The results in Fig. 11 and Table 4 indicated that when the stack ran for 120 h at 0.33 A cm⁻², the resistance of the interconnect was unchanged, the anodic CR increased by 0.0015 Ω cm², the resistance of the UC increased by 0.003 Ω cm² and the cathodic CR decreased by 0.007 Ω cm². Apparently, the decrease amplitude of the cathodic CR was larger than the sum of the anodic CR and the resistance of the UC. Therefore, the resistance of the whole SRU decreased, resulting in no degradation of the SRU. When the stack ran within 480 h in the constant current discharge of 0.44 A cm⁻², the resistance of the interconnect remained unchanged, the anodic CR increased by 0.00242 Ω cm², the resistance of the UC increased by 0.032 Ω cm² and the cathodic CR decreased by 0.005 Ω cm². Apparently, the increase amplitude of the anodic CR and the resistance of the UC were larger than that of the cathodic CR. Thus,

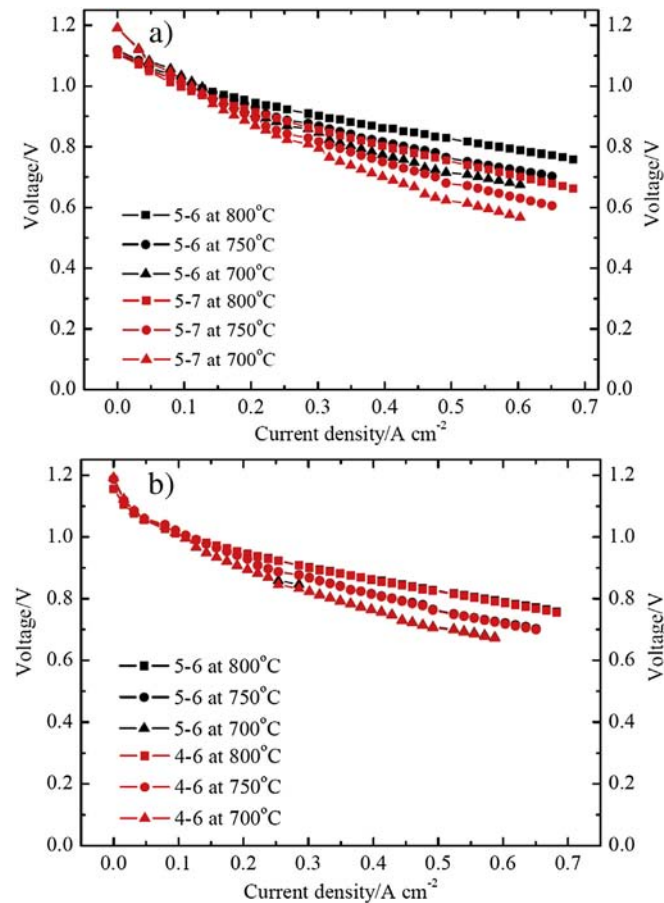**Fig. 8.** I−V curves between both ends of 5−6, 5−7 and 4−6: (a) both ends of 5−6 and 5−7 and (b) both ends of 5−6 and 4−6.
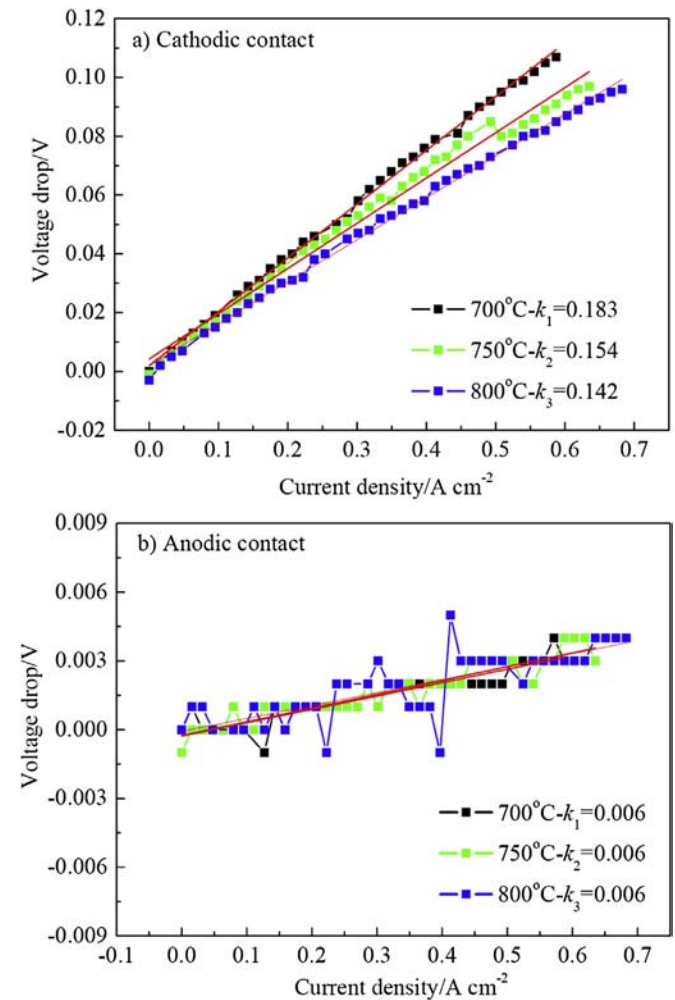

Fig. 9. Voltage drop of cathodic and anodic contact of the SRU 3# under different temperatures: (a) cathodic contact and (b) anodic contact.
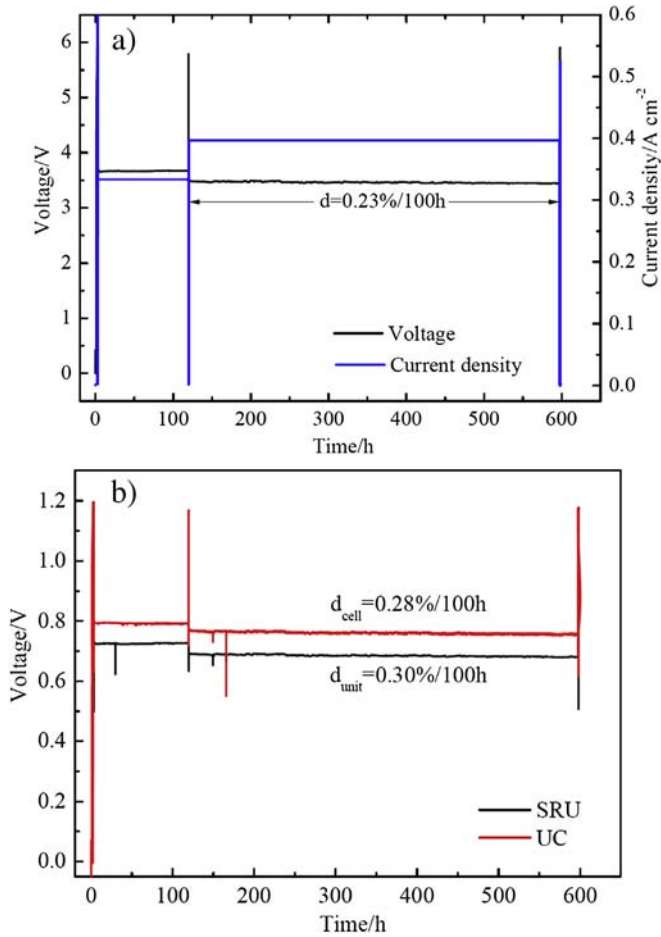
Fig. 10. V–t curve of the stack, SRU and UC under 700 °C: (a) stack and (b) SRU 3# and UC 3#.

decrease of the conductivity during the stack operation. Therefore, it was speculated that the agglomeration and growth of the Ni particles in the ACCL during the stack operation was the main reason for the continuous increase of the anodic resistance.

Fig. 14 is the SEM morphology of the cell cathode before and after the operation. The results indicated that the microstructure of the active cathode of the UC did not change significantly before and after the operation. Therefore, it was speculated that the increase of
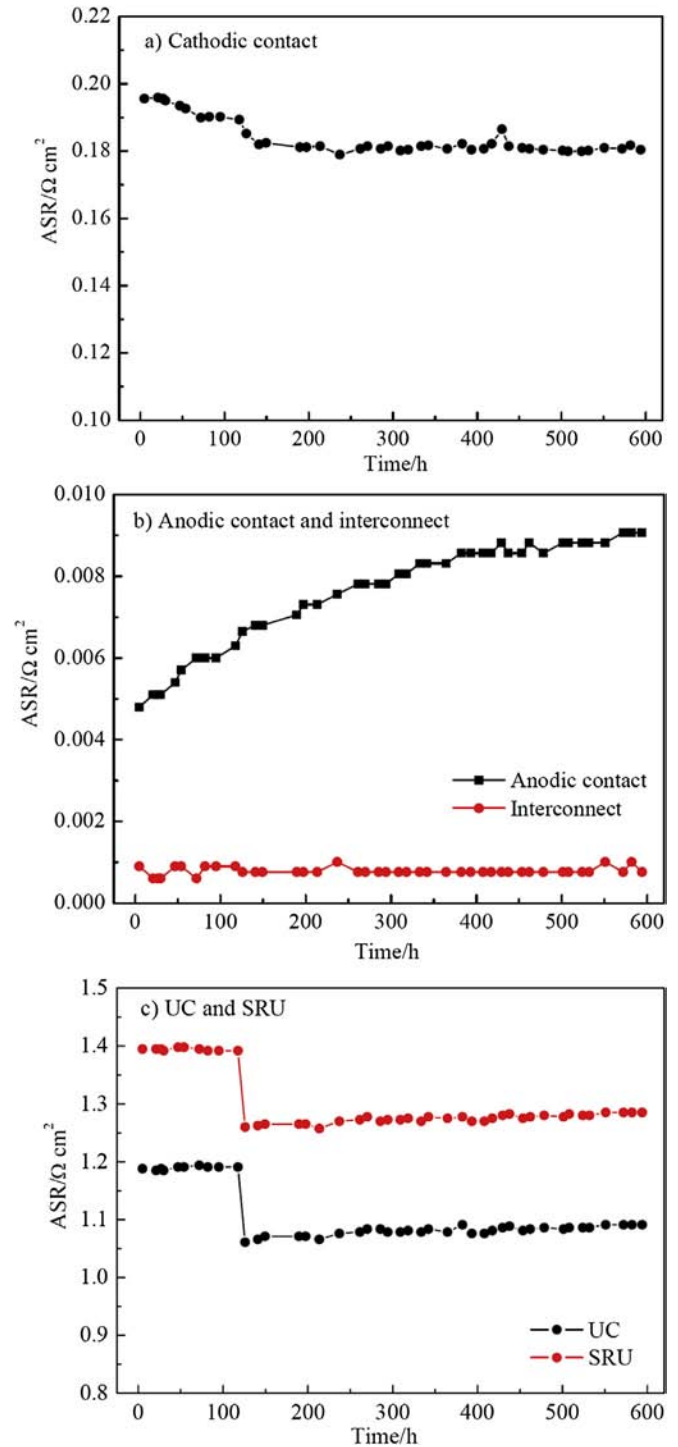
the resistance of the whole SRU increased, resulting in the degradation of the SRU.

Therefore, it was found that the increasing resistance of the UC was the main reason among the factors that caused the degradation of the SRU. The results listed in Table 4 also indicated that even though the initial value of the anodic CR was small, the increase rate of resistance was large. Thus, it was also a factor that influenced the stack degradation and could not be ignored. On the contrary to the anodic contact, the cathodic CR decreased and remained unchanged afterward. Therefore, the cathodic contact was not the main cause of the stack degradation.

Previous studies indicated [21] that when the cell cathode was in poor contact with the interconnect, the cathodic interfacial contact was the main reason for the stack degradation. However, the cathodic interfacial CR of this research always remained unchanged. Accordingly, it was not a factor of the stack degradation in this work. The phenomenon could be caused by the good contact of the interface. In this regard, the observation was conducted on the surface morphology of the CCCL on the UC. The results (shown in Fig. 12) indicated that the contact traces left by the metal interconnect on the CCCL surface were clear and even, showing good and even contact between the metal interconnect and the CCCL.

The observation with SEM was conducted on the ACCL in the stack, with the results shown in Fig. 13. After 600 h of constant current discharge, the Ni particles in the ACCL of the UC witnessed significant sintering and agglomeration. The reference [39] indicated that the agglomeration of Ni particles could cause the

Fig. 11. ASR of the components in the SRU 3#: (a) cathodic contact; (b) anodic contact and the interconnect and (c) the SRU and the UC.

Table 4
ASR of components of the SRU 3# at different times.

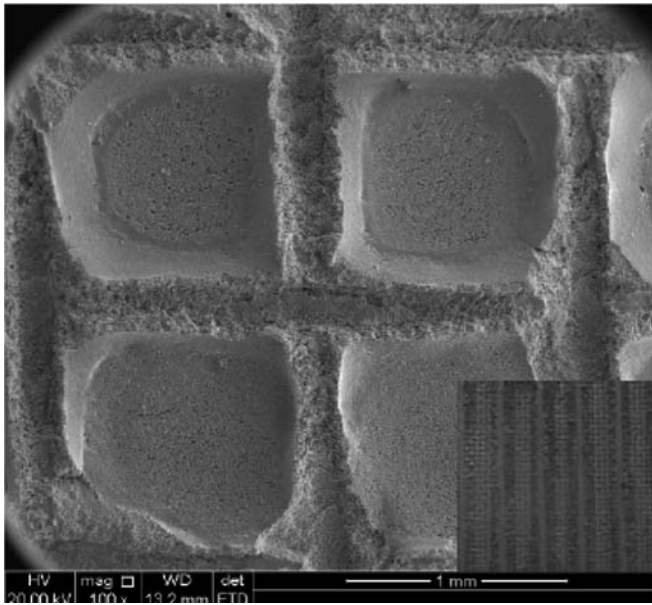| Operation time	0 h	120 h–0.33 A cm^{-2}	120 h–0.40 A cm^{-2}	600 h
Cathodic contact/Ω cm^2	0.196	0.189	0.185	0.180
Interconnect/Ω cm^2	0.0009	0.0009	0.000756	0.000756
Anodic contact/Ω cm^2	0.0048	0.0063	0.00665	0.00907
UC/Ω cm^2	1.188	1.191	1.061	1.093
SRU/Ω cm^2	1.395	1.392	1.260	1.285

Fig. 12. Morphology of the CCCL on the UC after testing.

the cell resistance was scarcely influenced by the active cathode. The observations with SEM and EDS were conducted on the supported anode section before and after the constant current discharge, as shown in Fig. 15. In comparison with the anode microstructure before operation, it was found that the Ni particles were sintered, agglomerated and densified after the operation. This could be the factor that caused the cell degradation.

In order to testify the results above, the energy spectral analysis was conducted on the anode before and after the operation. The results are shown in Fig. 16. The results indicated that the

distribution of Ni particle was even before the operation, but grew bigger after the operation. Literature reported [39] that the agglomeration of Ni particles induced the increase of the resistance rate. Further SEM analysis on the electrolyte section before and after the operation (Fig. 17) indicated that the electrolyte section of the UC was intact before the operation, while after discharge it showed clear cracks. This led to the increase of the cell resistance and the cell degradation. During the discharge, the reason for the crack formation of electrolyte and the sources of the variation of the electrode resistance and the electrolyte resistance require further studies.

4. Conclusion

Quantitative investigation was conducted on the resistance sources of the components in the Ni-YSZ/YSZ/LCF-YSZ SOFC stack. The stack was assembled by using SUS 430 as metal interconnect and Al$_2$O$_3$–SiO$_2$–CaO-based glass as the sealing material. The results indicated that in the SRU, at the temperature of 700 °C, 750 °C and 800 °C, the ASR of the SRU was 0.915 Ω cm^2, 0.717 Ω cm^2 and 0.492 Ω cm^2, respectively. The cell ASR was 0.729 Ω cm^2, 0.556 Ω cm^2 and 0.345 Ω cm^2, respectively, accounting for, 79.7%, 77.5% and 70.1% of that of the SRU. The UC was the main factor that influenced the stack performance. Under the previously stated temperature, the cathode CR in the SRU was 0.183 Ω cm^2, 0.154 Ω cm^2 and 0.142 Ω cm^2, respectively, accounting for 20.0%, 21.5% and 28.9% of the total resistance of the SRU, which was the second factor that influenced the performance of the stack. The results indicated that the anode CR in the SRU was 0.006 Ω cm^2, accounting for approximately 0.6%, 0.8% and 1.2% of the whole unit in the stack. The resistance of the interconnect was small and could be neglected. However, the results indicated that the performance of the SRU was influenced by the cell itself and the cathode CR, accounting for 70.1–79.7% and 20.0–28.9%, respectively. The performance was basically irrelevant with the anode contact and the interconnect.

The constant current discharge revealed that the degradation rate of the SRU and the UC was 0.3%/100 h and 0.28%/100 h, respectively. The degradation rate of the UC accounted for about 93.3% of that of the SRU. When the stack ran for 120 h at 0.33 A cm^{-2}, the resistance of the interconnect did not vary, the anodic CR increased by 0.0015 Ω cm^2, the cell resistance increased by 0.003 Ω cm^2, and the cathodic CR decreased by 0.007 Ω cm^2. The decrease amplitude of the cathodic CR was larger than the sum of that of the increase of the anodic CR and the cell resistance.
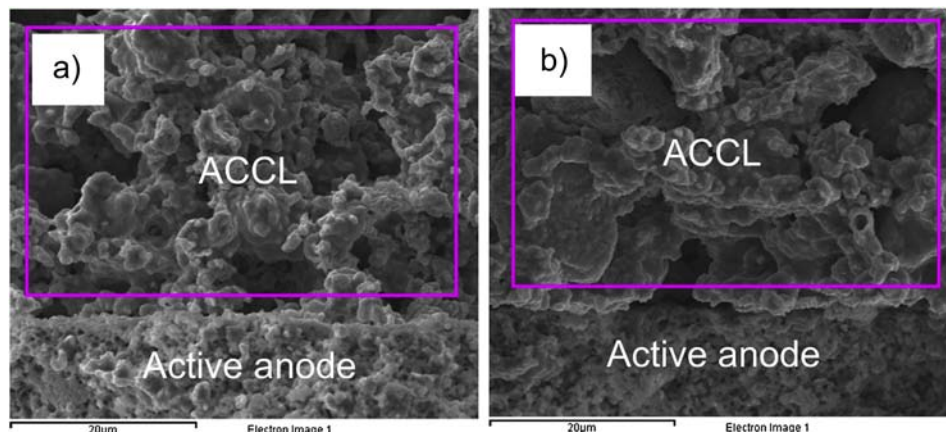

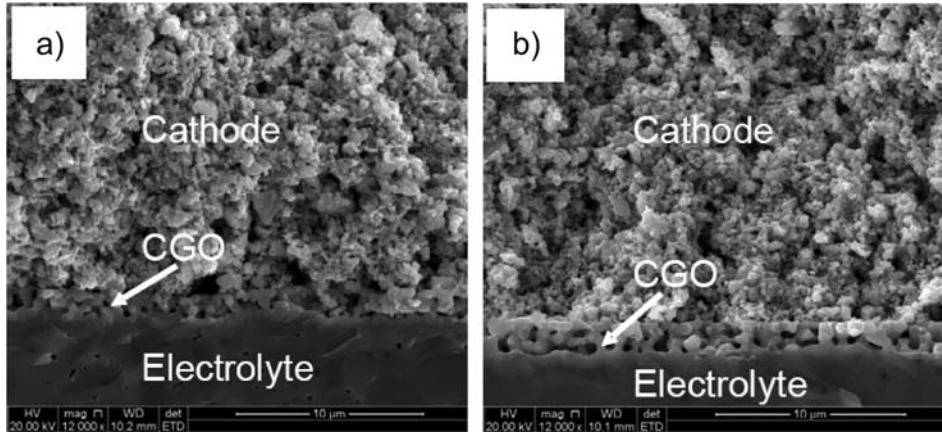**Fig. 13.** Section morphology of the ACCL on the UC: (a) before discharge and (b) after discharge.

Fig. 14. SEM morphology of cell cathode before and after the operation: (a) before the operation and (b) after the operation.
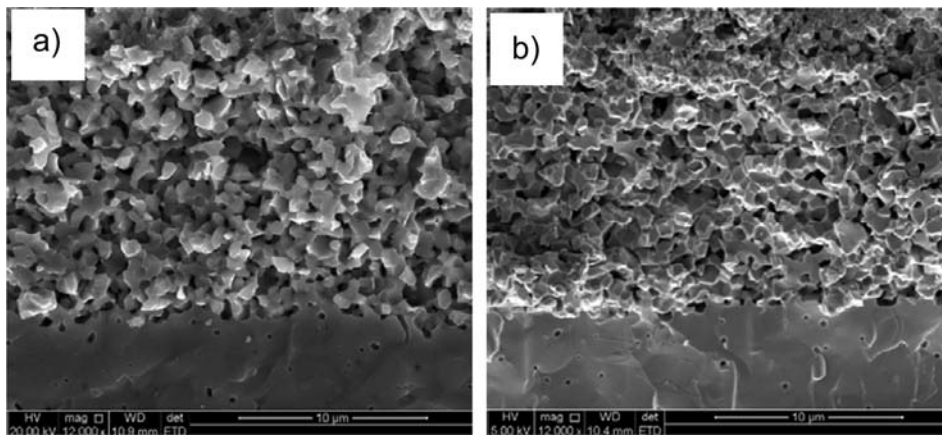

Fig. 15. Anodic section: (a) before constant current discharge and (b) after constant current discharge.

Therefore, at the constant current discharge of 0.33 A cm^{-2}, the resistance of the whole SRU decreased, thus the SRU did not degrade. When the stack ran for 480 h at the constant current discharge of 0.40 A cm^{-2}, the resistance of the interconnect remained unchanged, the anodic CR increased by 0.00242 Ω cm^2, the cell resistance increased by 0.032 Ω cm^2, and the cathodic CR decreased by 0.005 Ω cm^2. Therefore, the increasing resistance of the whole SRU caused its degradation. Therefore, the increase of the
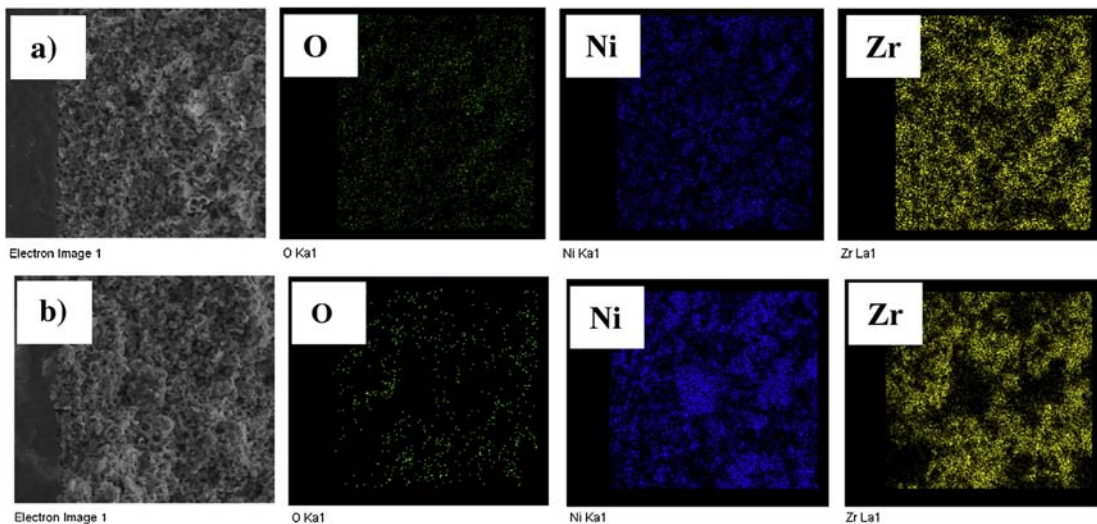

Fig. 16. Anodic section EDS before and after discharge: (a) before discharge and (b) after discharge.
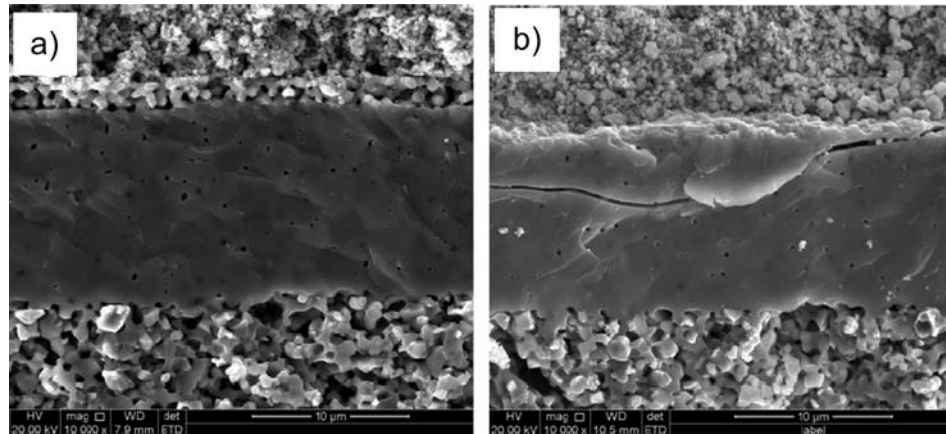
Fig. 17. Electrolyte section SEM before and after the discharge operation: (a) before discharge and (b) after discharge.

cell resistance itself was the main reason for the degradation of the SRU. In addition, the anodic CR was the factor influencing the stack degradation that could not be neglected due to rapid increasing for long-time operation. Different from the anode contact, the cathodic CR decreased and then remained unchanged. Therefore, when the cell cathode contacts the interconnect well, the cathodic contact was not the cause of the stack degradation.

Acknowledgment

References

[1] T.L. Wen, D. Wang, H.Y. Tu, M. Chen, Z. Lu, Z. Zhang, H. Nie, W. Huang, Solid State Ionics 152–153 (2002) 399–404.
[2] H.Y. Tu, U. Stimming, J. Power Sources 127 (2004) 284–293.
[3] L. Barelli, E. Barluzzi, G. Bidini, Int. J. Hydrogen Energy 38 (2013) 5060–5074.
[4] J.I. Gazzarri, O. Kesler, J. Power Sources 167 (2007) 430–441.
[5] J.I. Gazzarri, O. Kesler, J. Power Sources 167 (2007) 100–110.
[6] A.V. Virkar, J. Power Sources 172 (2007) 713–724.
[7] H. Lim, A.V. Virkar, J. Power Sources 185 (2008) 790–800.
[8] P. Batfalsky, V.A.C. Haanappel, J. Malzbender, N.H. Menzler, V. Shemet, I.C. Vinke, R.W. Steinbrech, J. Power Sources 155 (2006) 128–137.
[9] F. Smeacetto, M. Salvo, M. Santarelli, P. Leone, G.A. Ortigoza-Villalba, A. Lanzini, L.C. Ajitdoss, M. Ferraris, Int. J. Hydrogen Energy 38 (2013) 588–596.
[10] W.G. Wang, W.B. Guan, H.M. Li, Y.J. Xue, J.X. Wang, Y.N. Wu, J. Wang, K. Liu, SOFC Research and Development at NIMTE, B0404 – Abstract 236 – Oral Presentation – Session B04 – Innovative Applications and Designs, Tuesday, July 1, 2008.
[11] K. Wanga, D. Hissel, M.C. Péra, N. Steiner, D. Marra, M. Sorrentino, C. Pianese, M. Monteverde, P. Cardone, J. Saarinen, Int. J. Hydrogen Energy 36 (2011) 7212–7228.
[12] F. Smeacetto, M. Salvo, P. Leone, M. Santarelli, M. Ferraris, Mater. Lett. 65 (2011) 1048–1052.
[13] S.F. Wang, Y.F. Hsu, H.C. Lu, S.C. Lo, C.S. Cheng, Int. J. Hydrogen Energy 37 (2012) 5901–5913.
[14] S.D. Song, M. F Han, J.Q. Zhang, H. Fan, J. Power Sources 233 (2013) 62–68.
[15] L.D. Fan, C.Y. Wang, M.M. Chen, B. Zhu, J. Power Sources 234 (2013) 154–174.
[16] O. Thomann, M. Pihlatie, M. Rautanen, O. Himanen, J. Lagerbom, M. Makinen, T. Varis, T. Suhonen, J. Kiviahocts, J. Therm. Spray Technol. 22 (2013) 631–639.
[17] J.W. Stevenson, Z.G. Yang, G.G. Xia, Z. Nie, J.D. Templeton, J. Power Sources 231 (2013) 256–263.
[18] S. Fontana, S. Chevalier, G. Caboche, Oxid. Met. 78 (2012) 307–328.
[19] J.V. herle, D. Perednis, K. Nakamura, S. Diethelm, M. Zahid, A. Aslanides, T. Somekawa, Y. Baba, K. Horiuchi, Y. Matsuzaki, M. Yoshimoto, O. Bucheli, J. Power Sources 182 (2008) 389–399.
[20] D. Larrain, J.V. herle, D. Favrat, J. Power Sources 161 (2006) 392–403.
[21] W.B. Guan, L. Jin, X. Ma, W.G. Wang, Fuel Cells 12 (2012) 1085–1094.
[22] L. Jin, W.B. Guan, J.Q. Niu, X. Ma, W.G. Wang, J. Power Sources 240 (2013) 796–805.
[23] L.G.J. de Haart, J. Mougin, O. Posdziech, J. Kiviaho, N.H. Menzler, Fuel Cells 9 (2009) 794–804.
[24] J. Malzbender, P. Batfalsky, R. Vaßen, V. Shemet, F. Tietz, J. Power Sources 201 (2012) 196–203.
[25] S. Fontana, S. Chevalier, G. Caboche, Mater. Corros. 62 (2011) 650–658.
[26] K.A. Nielsen, A.R. Dinesen, L. Korcakova, L. Mikkelsen, P.V. Hendriksen, F.W. Poulsen, Fuel Cells 06 (2006) 100–106.
[27] A. Moran-Ruiz, K. Vidal, A. Larranaga, Fuel Cells 13 (2013) 398–403.
[28] T. Dey, D. Singdeo, M. Bose, R.N. Basu, P.C. Ghosh, J. Power Sources 233 (2013) 290–298.
[29] W. Wu, G.L. Wang, W.B. Guan, Y.F. Zheng, W.G. Wang, Fuel Cells 13 (2013) 743–750.
[30] H.T. Lim, S.C. Hwang, M.G. Jung, H.W. Park, M.Y. Park, S.S. Lee, Y.G. Jung, Fuel cells 13 (2013) 712–719.
[31] J.H. Choi, T. Lee, M. Choi, Y.S. Yoo, S.W. Baek, J. Bae, Int. J. Hydrogen Energy 35 (2010) 4285–4291.
[32] Y.C. Hsiao, J.R. Selman, Solid State Ionics 98 (1997) 33–38.
[33] W.B. Guan, H.J. Zhai, L. Jin, C. Xu, W.G. Wang, Fuel Cells 12 (2012) 24–31.
[34] W.B. Guan, L. Jin, W. Wu, Y.F. Zheng, G.L. Wang, W.G. Wang, J. Power Sources 245 (2013) 119–128.
[35] D. Penchini, G. Cinti, G. Discepoli, E. Sisani, U. Desideri, Int. J. Hydrogen Energy 38 (2013) 525–531.
[36] A.C. Burt, I.B. Celik, R.S. Gemmen, A.V. Smirnov, J. Power Sources 126 (2004) 76–87.
[37] N. Watanabe, T. Ooe, Y. Akagi, T. Ishihara, Int. J. Hydrogen Energy 37 (2012) 8562–8571.
[38] J.X. Wang, Y.K. Tao, J. Shao, W.G. Wang, J. Power Sources 186 (2009) 344–348.
[39] D. Simwonis, F. Tietz, D. Stöver, Solid State Ionics 132 (2000) 241–251.